Proceedings of the Seventeenth International Conference on
Civil, Structural and Environmental Engineering Computing
Edited by: P. Iványi, J. Kruis and B.H.V. Topping
Civil-Comp Conferences, Volume 6, Paper 2.7
Civil-Comp Press, Edinburgh, United Kingdom, 2023
doi: 10.4203/ccc.6.2.7

Identification torsional-flexural frequencies for thin-wall beams from the rocking motion of a two-wheel test vehicle

K. Shi, X.Q. Mo, H. Xu, Z.L. Wang and Y.B. Yang

School of Civil Engineering, Chongqing University
Chongqing, China

Abstract

This paper proposes a furthering approach for extracting the first several *flexural* and *torsional-flexural* frequencies of thin-walled box girders from the residual contact response of a two-wheel test vehicle passing the bridge. Unlike most previous studies, the single-axle test vehicle is modeled as a *two degree-of-freedom* (DOF) system to account for the two wheels' rocking motion, which relates to torsional-flexural motion of the beam. To start, a new theory for the mono-symmetric thin-walled beam subjected to a two-wheel moving vehicle is presented. The *wheel contact response* derived herein (which is free of vehicle frequencies) enables us in the first stance to remove the overshadowing effect on bridge frequencies brought by outstanding vehicle frequencies. The other concern in extracting the bridge frequencies is the noises posed by random pavement roughness, which is overcome through the use of the *residual contact response* generated by two identical connected vehicles. This paper furthers the existing ones in that the wheel response (i.e. the vehicle's rocking motion) is utilized to extract the torsional-flexural frequencies of the bridge, making use of the linking action between the vehicle's two wheels and the bridge's cross section.

Keywords: torsional-flexural frequency, thin-wall beam, contact point, moving vehicle, vehicle scanning method

1 Introduction

Using the modal parameters, such as frequency, mode shape, damping ratio and others, to assess the health condition of a bridge has been widely accepted in engineering practice [1-4]. Previously, measurement methods using fixed sensors have been conducted for bridges to obtain their modal properties via the use of excitation sources such as ambient vibrations, forced vibrations, impact vibrations, etc. These methods are referred to as the direct approach, as they rely on the collection of vibration data generated by a network of sensors directly deployed on the bridge. Such an approach was often blamed for issues such as the high cost and labor required in installation and maintenance, the huge amount of daily generated data that can hardly be efficiently treated, and the relatively short lifespans of sensing devices compared with the bridge to be monitored. Moreover, the high cost of deployment has prohibited the direct approach from being applied to bridges of medium- and small-spans. This has presented a threat to the overall health monitoring of highway or railway networks, as the majority of medium- and small-span bridges that are not monitored constitute the major parts of each network. Clearly, a rapid measurement approach using speedy and mobile techniques for bridges is all that is needed to meet the need of the tremendous amount of bridges worldwide.

Aimed at tackling the problems mentioned above, the vehicle scanning method (VSM) or indirect approach that utilizes a moving test vehicle to extract the dynamic properties of the bridge was proposed in 2004 [5,6]. Based on vehicle-bridge interaction (VBI), the dynamic properties of a bridge, e.g., frequencies, damping ratios and mode shapes, etc., can be identified from the response recorded of an instrumented test vehicle during its passage over the bridge. Because of the obvious advantages of mobility, economy, and efficiency, the VSM has attracted the attention of researchers worldwide. In less than two decades, an awful amount of works has been conducted on the identification of various properties of bridges, such as frequencies, damages, modal shapes, damping ratios, time-varying parameters, to name a few. The application of this method has also been demonstrated in a number of model and field tests.

Previously, the single-axle test vehicle was modelled as a single degree-of-freedom (DOF) system for its simplicity and resemblance with the underlying theory. In fact, the single-axle test vehicle contains two wheels and one axle. The two wheels will behave in the form of rocking motion when they are differentially excited, i.e., when passing paths of uneven surfaces. To accommodate such an effect, a more realistic approach is to treat the two wheels each as one DOF system, and connected by a rigid axle. With this, both the rocking and vertical motions can be duly captured. In this paper, the rocking motion of the two-wheel test vehicle will be exploited to extract the torsional-flexural frequencies of the thin-walled beams.

To meet the goal described above, a new theory will be presented for a mono-symmetric thin-walled beam subjected to the moving test vehicle with two wheels.

Closed-form solutions will be derived for the vehicle, beam and wheel contact responses. The noisy surface roughness effect will be eliminated by using the residual contact response of two connected identical vehicles, rather than the original single vehicle response.

2 Theoretical derivations

To be more realistic, the single-axle test vehicle will be modelled as a *damped two-DOF* system to consider both the vertical (y_v) and rocking (θ_v) motions of the two wheels in this study. The axle is assumed to be *rigid* and fitted with three sensors, one at the centre and the other two at locations close to the two wheels; the latter will be referred to as *wheel sensors*. Based on Vlasov's hypothesis, a thin-walled box girder of length L_0 is modelled as a one-dimensional beam acted upon by the vehicle with two wheels moving at speed V, as shown in Figure 1, where the shear centre S is separate from the centroid C. The origin of the coordinate system is located at the centroid C, but the responses of the thin-walled beam are measured with respect to the shear centre S. For the mono-symmetric beam in Figure 1, the lateral and torsional vibrations are coupled, while the flexural (vertical) vibration is uncoupled. To facilitate derivation of the new, closed-form solutions, the damping of the beam is neglected, but will be included in the numerical study later on.

Based on Vlasov's theory of thin-walled beams, the *vertical*, *lateral* and *torsional* equations of motion of the beam under the damped 2-DOF moving vehicle can be respectively given as follows:

$$EI_z v''''(x,t) + m\ddot{v}(x,t) = F_c^L(t)\delta(x-Vt) + F_c^R(t)\delta(x-Vt) \tag{1}$$

$$EI_y w''''(x,t) + m\ddot{w}(x,t) + m\eta\ddot{\theta}(x,t) = 0 \tag{2}$$

$$\begin{aligned} &EI_\omega \theta''''(x,t) - GJ\theta''(x,t) + m\left(\eta^2 + r^2\right)\ddot{\theta}(x,t) + m\eta\ddot{w}(x,t) \\ &= e^L F_c^L(t)\delta(x-Vt) + e^R F_c^R(t)\delta(x-Vt) \end{aligned} \tag{3}$$

where $v(x,t)$, $w(x,t)$ and $\theta(x,t)$ denote the vertical, lateral and torsional displacements, respectively, of the beam; an overdot ($\dot{}$) and prime ( )' denote the derivative with respect to time t and axis x, respectively; δ is Dirac's delta function; e_0, e^R, e^L respectively denote the eccentricities of the central, right and left sensors from the centroid C, $e^R = e_0 + l_0/2$, $e^L = e_0 - l_0/2$; and $F_c^L(t)$ and $F_c^R(t)$ respectively the right and left contact forces,

$$F_c^L(t) = \frac{m_v g + k_v\left(y_v(t) - \theta_v(t)l_0/2 - u_c^L(t)\right) + c_v(\dot{y}_v(t) - l_0\dot{\theta}_v(t)/2 - \dot{u}_c^L(t))}{2} \tag{4}$$

$$F_c^R(t) = \frac{m_v g + k_v\left(y_v(t) + \theta_v(t)l_0/2 - u_c^R(t)\right) + c_v(\dot{y}_v(t) + l_0\dot{\theta}_v(t)/2 - \dot{u}_c^R(t))}{2} \tag{5}$$

The equations for the vertical and rocking motions of the vehicle are

$$m_v\ddot{y}_v(t)+c_v\dot{y}_v(t)+k_v y_v(t)=k_v\frac{u_c^L(t)+u_c^R(t)}{2}+c_v\frac{\dot{u}_c^L(t)+\dot{u}_c^R(t)}{2} \tag{6}$$

$$J_v\ddot{\theta}_v(t)+\frac{l_0^2c_v}{4}\dot{\theta}_v(t)+\frac{l_0^2k_v}{4}\theta_v(t)=\frac{l_0^2c_v}{4}\frac{(\dot{u}_c^R(t)-\dot{u}_c^L(t))}{l_0}+\frac{l_0^2k_v}{4}\frac{(u_c^R(t)-u_c^L(t))}{l_0} \tag{7}$$

where $u_c^R(t)$ and $u_c^L(t)$ are the displacements of the contact points of the right and left wheels, respectively; and g the acceleration of gravity. Other parameters in Eqs. (1)-(7) are given as follows: For the vehicle, V = moving speed, k_v = stiffness coefficient, c_v = damping coefficient, J_v = mass moment of inertia, m_v = mass, l_0 = distance between two wheels (or sensors); and for the beam, (E, G) = elastic and shear moduli, (I_z, I_y) = moments of inertia about the z- and y-axis, I_ω = warping constant, J = torsional moment of inertia, m = mass per unit length, η = offset between S and C along the y-axis, and r = polar radius of gyration.

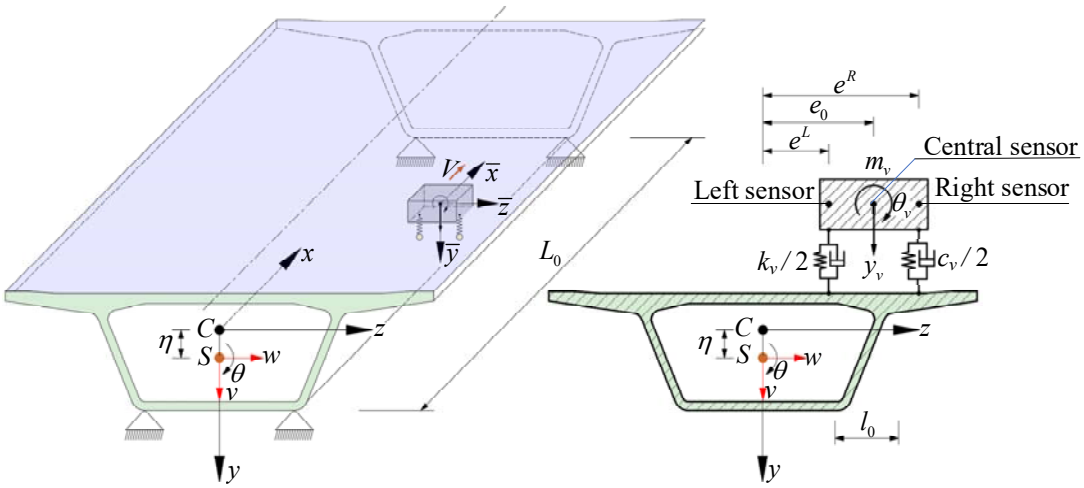

(a) (b)

Figure 1. Vehicle-bridge model: (a) perspective view, (b) profile view.

In practice, both the lateral and torsional displacements are prevented by diaphragms and the vertical displacement by end bearings of the thin-walled beam, but the end cross sections are free to warp. For the problem considered, the boundary conditions are:

$$v(0,t)=v(L_0,t)=0,\quad v''(0,t)=v''(L_0,t)=0 \tag{8}$$

$$w(0,t)=w(L_0,t)=0,\quad w''(0,t)=w''(L_0,t)=0 \tag{9}$$

$$\theta(0,t)=\theta(L_0,t)=0,\quad \theta''(0,t)=\theta''(L_0,t)=0 \tag{10}$$

and the initial conditions are

$$v(x,0)=0,\quad \dot{v}(x,0)=0 \tag{11}$$

$$w(x,0)=0,\quad \dot{w}(x,0)=0 \tag{12}$$

$$\theta(x,0)=0\,,\quad \dot{\theta}(x,0)=0 \tag{13}$$

For the boundary conditions in Eqs. (8)-(10), the displacements of the beam can be approximated as:

$$w(x,t)=\sum_{n=1}^{\infty}Z_n(t)\sin(\frac{n\pi x}{L_0})\,,\ v(x,t)=\sum_{n=1}^{\infty}Y_n(t)\sin(\frac{n\pi x}{L_0})\,,\quad \theta(x,t)=\sum_{n=1}^{\infty}\Theta_n(t)\sin(\frac{n\pi x}{L_0}) \tag{14a-c}$$

where $Z_n(t)$, $Y_n(t)$ and $\Theta_n(t)$ denote the n-th modal coordinates. It should be noted that approximate functions given in Eqs. (14) meet the condition of *admissibility* required in mechanics formulation. The sinusoidal functions are only used to express the *variation* of *each* displacement component between the two boundary ends. The torsional-flexural coupling is still there, as can be seen from the modal equations to follow. Besides, the accuracy of this approximation will be validated independently by the finite element method (FEM).

Substituting Eqs. (14a-c) into Eqs. (1)-(3), multiplying both sides by $\sin(n\pi x/L_0)$, integrating with respect to x from 0 to L_0, and using the property for the Dirac's delta function $\int_{-\infty}^{+\infty}f(x)\delta(x-x_0)dx=f(x_0)$ and the orthogonality conditions for trigonometric functions, one can arrive at the following modal equations for the thin-walled beam:

$$\ddot{Y}_n(t)+\omega_{yn}^2Y_n(t)=\frac{2(F_c^L(t)+F_c^R(t))}{mL_0}\sin(\frac{n\pi Vt}{L_0}) \tag{15}$$

$$\ddot{Z}_n(t)+\omega_{zn}^2Z_n(t)+\eta\ddot{\Theta}_n(t)=0 \tag{16}$$

$$\ddot{\Theta}_n(t)+\omega_{\theta n}^2\Theta_n(t)+\frac{\eta}{\eta^2+r^2}\ddot{Z}_n(t)=\frac{2\left[e^LF_c^L(t)+e^RF_c^R(t)\right]}{m(\eta^2+r^2)L_0}\sin(\frac{n\pi Vt}{L_0}) \tag{17}$$

By defining the n-th modal flexural, lateral, and torsional frequencies of the beam as

$$\omega_{yn}^2=\frac{EI_z(n\pi)^4}{mL_0^4}\,,\ \omega_{zn}^2=\frac{EI_y(n\pi)^4}{mL_0^4}\,,\ \omega_{\theta n}^2=\frac{GJ(n\pi L_0)^2+EI_\omega(n\pi)^4}{m(\eta^2+r^2)L_0^4} \tag{18a-c}$$

and assuming the vehicle mass to be far smaller than the bridge's, i.e., $m_v<<mL_0$, the modal equations of the beam reduce to

$$\ddot{Y}_n(t)+\omega_{yn}^2Y_n(t)=\frac{2m_vg}{mL_0}\sin(\frac{n\pi Vt}{L_0}) \tag{19}$$

$$\ddot{Z}_n(t)+\omega_{zn}^2Z_n(t)+\eta\ddot{\Theta}_n(t)=0 \tag{20}$$

$$\ddot{\Theta}_n(t)+\omega_{\theta n}^2\Theta_n(t)+\frac{\eta}{\eta^2+r^2}\ddot{Z}_n(t)=\frac{2e_0m_vg}{m(\eta^2+r^2)L_0}\sin(\frac{n\pi Vt}{L_0}) \tag{21}$$

In the following, the coupled lateral $w(x,t)$ and torsional $\theta(x,t)$ displacements will be solved first. Letting $Z_n(t) = P_n e^{i\omega_n t}$, $\Theta_n(t) = Q_n e^{i\omega_n t}$, one can derive from Eqs. (20) and (21) the homogeneous equations for the lateral and torsional motions:

$$\left(\omega_n^2 - \omega_{zn}^2\right) P_n + \eta Q_n \omega_n^2 = 0 \tag{22}$$

$$\left(\omega_n^2 - \omega_{\theta n}^2\right) Q_n + \frac{\eta}{\eta^2 + r^2} \omega_n^2 P_n = 0 \tag{23}$$

or

$$\begin{bmatrix} \omega_n^2 - \omega_{zn}^2 & \eta\omega_n^2 \\ \dfrac{\eta}{\eta^2 + r^2}\omega_n^2 & \omega_n^2 - \omega_{\theta n}^2 \end{bmatrix} \begin{Bmatrix} P_n \\ Q_n \end{Bmatrix} = \begin{Bmatrix} 0 \\ 0 \end{Bmatrix} \tag{24}$$

For nontrivial solution, the determinant of the above matrix should be zero, i.e.,

$$(1-\alpha)\omega_n^4 - \left(\omega_{zn}^2 + \omega_{\theta n}^2\right)\omega_n^2 + \omega_{zn}^2 \omega_{\theta n}^2 = 0 \tag{25}$$

where the offset parameter α is defined as

$$\alpha = \frac{\eta^2}{\eta^2 + r^2} \tag{26}$$

From the fourth-order polynomial Eq. (25), the n-th dual frequencies can be solved as

$$\omega_{n^-}^2 = \frac{\left(\omega_{zn}^2 + \omega_{\theta n}^2\right) - \sqrt{\left(\omega_{zn}^2 - \omega_{\theta n}^2\right)^2 + 4\alpha\omega_{zn}^2\omega_{\theta n}^2}}{2(1-\alpha)} \tag{27a}$$

$$\omega_{n^+}^2 = \frac{\left(\omega_{zn}^2 + \omega_{\theta n}^2\right) + \sqrt{\left(\omega_{zn}^2 - \omega_{\theta n}^2\right)^2 + 4\alpha\omega_{zn}^2\omega_{\theta n}^2}}{2(1-\alpha)} \tag{27b}$$

The two frequencies ω_{n^-} and ω_{n^+} are conjugate, representing the low- and high-frequency components, respectively, of the torsional-flexural motion. In this study, the frequency ω_{n^-} is called the n-th "minus" torsional-flexural frequency, and ω_{n^+} the n-th "plus" one. For bisymmetric cross sections, i.e., with the offset α = 0, the above frequencies will reduce to those commonly known.

To solve the coupling Eqs. (20) and (21), one can transform them into the s-domain by the Laplace transformation. For null initial conditions, $Z_n(0) = 0$, $\dot{Z}_n(0) = 0$, $\Theta_n(0) = 0$ and $\dot{\Theta}_n(0) = 0$, the transformed equations are

$$\left(s^2 + \omega_{zn}^2\right)\bar{Z}_n(s) + s^2\eta\bar{\Theta}_n(s) = 0 \tag{28}$$

$$\left(s^2 + \omega_{\theta n}^2\right)\bar{\Theta}_n(s) + \frac{s^2\eta}{\eta^2 + r^2}\bar{Z}_n(s) = \frac{2e_0 m_v g \Omega_n}{mL_0(\eta^2 + r^2)(\Omega_n^2 + s^2)} \tag{29}$$

where $\bar{Z}_n(s)$ and $\bar{\Theta}_n(s)$ respectively denote the Laplace transforms of $Z_n(t)$ and $\Theta_n(t)$.

The solutions to Eqs. (28) and (29) are

$$\bar{Z}_n(s) = -\frac{2\Omega_n \eta s^2 e_0 m_v g}{mL_0 r^2 \left(s^2+\Omega_n^2\right)\left(s^2+\omega_{n^-}^2\right)\left(s^2+\omega_{n^+}^2\right)} \tag{30}$$

$$\bar{\Theta}_n(s) = \frac{2\Omega_n e_0 m_v g(s^2+\omega_{yn}^2)}{mL_0 r^2 \left(s^2+\Omega_n^2\right)\left(s^2+\omega_{n^-}^2\right)\left(s^2+\omega_{n^+}^2\right)} \tag{31}$$

where Ω_n is the speed parameter,

$$\Omega_n = \frac{n\pi V}{L_0} \tag{32}$$

The time-domain expression for Eq. (30) is

$$Z_n(t) = A_{1n}\sin\Omega_n t + A_{2n}\sin\omega_{n^-}t + A_{3n}\sin\omega_{n^+}t \tag{33}$$

in which

$$A_{1n} = \varepsilon\Omega_n\left(\omega_{n^-}^2-\omega_{n^+}^2\right),\ A_{2n} = \varepsilon\omega_{n^-}\left(\omega_{n^+}^2-\Omega_n^2\right),\ A_{3n} = -\varepsilon\omega_{n^+}\left(\omega_{n^-}^2-\Omega_n^2\right) \tag{34a-c}$$

and

$$\varepsilon = \frac{2\eta e_0 m_v g\Omega_n}{r^2 mL_0\left(\omega_{n^-}^2-\omega_{n^+}^2\right)\left(\omega_{n^-}^2-\Omega_n^2\right)\left(\omega_{n^+}^2-\Omega_n^2\right)} \tag{35}$$

In a similar way, the time-domain expression for Eq. (31) is

$$\Theta_n(t) = B_{1n}\sin\Omega_n t + B_{2n}\sin\omega_{n^-}t + B_{3n}\sin\omega_{n^+}t \tag{36}$$

in which

$$B_{1n} = \frac{A_{1n}}{\eta}\left(\frac{\omega_{zn}^2}{\Omega_n^2}-1\right),\ B_{2n} = \frac{A_{2n}}{\eta}\left(\frac{\omega_{zn}^2}{\omega_{n^-}^2}-1\right),\ B_{3n} = \frac{A_{3n}}{\eta}\left(\frac{\omega_{zn}^2}{\omega_{n^+}^2}-1\right) \tag{37a~c}$$

With the use of Eqs. (33) and (36), the lateral and torsional displacements of the beam can be obtained from Eqs. (14b) and (14c) as

$$w(x,t) = \sum_{n=1}^{\infty}\left(A_{1n}\sin\Omega_n t + A_{2n}\sin\omega_{n^-}t + A_{3n}\sin\omega_{n^+}t\right)\sin(\frac{n\pi x}{L_0}) \tag{38}$$

$$\theta(x,t) = \sum_{n=1}^{\infty}\left(B_{1n}\sin\Omega_n t + B_{2n}\sin\omega_{n^-}t + B_{3n}\sin\omega_{n^+}t\right)\sin(\frac{n\pi x}{L_0}) \tag{39}$$

The vertical response $v(x,t)$ is independent of the torsional-flexural motion, which can be solved as:

$$v(x,t) = \sum_{n=1}^{\infty} C_n\left(\sin\Omega_n t - S_n\sin\omega_{yn}t\right)\sin(\frac{n\pi x}{L_0}) \tag{40}$$

where

$$\Delta_{stn} = \frac{2m_v g L_0^3}{EI_z n^4\pi^4},\ S_n = \frac{n\pi V}{L_0\omega_{yn}},\ C_n = \frac{\Delta_{stn}}{1-S_n^2} \tag{41a-c}$$

3 Results

The FEM is used to verify the reliability of the theory newly presented in Section 2. For the bridge midspan, the lateral, vertical and torsional displacements

computed analytically using 30 modes were compared with the FEM results in Figures. 2(a)-(c), respectively. Clearly, excellent agreement has been achieved between the analytical and numerical solutions. For the vehicle and contact responses, it goes without saying that excellent agreement has also been achieved between the analytical and numerical solutions. But they were omitted to save the paper length.

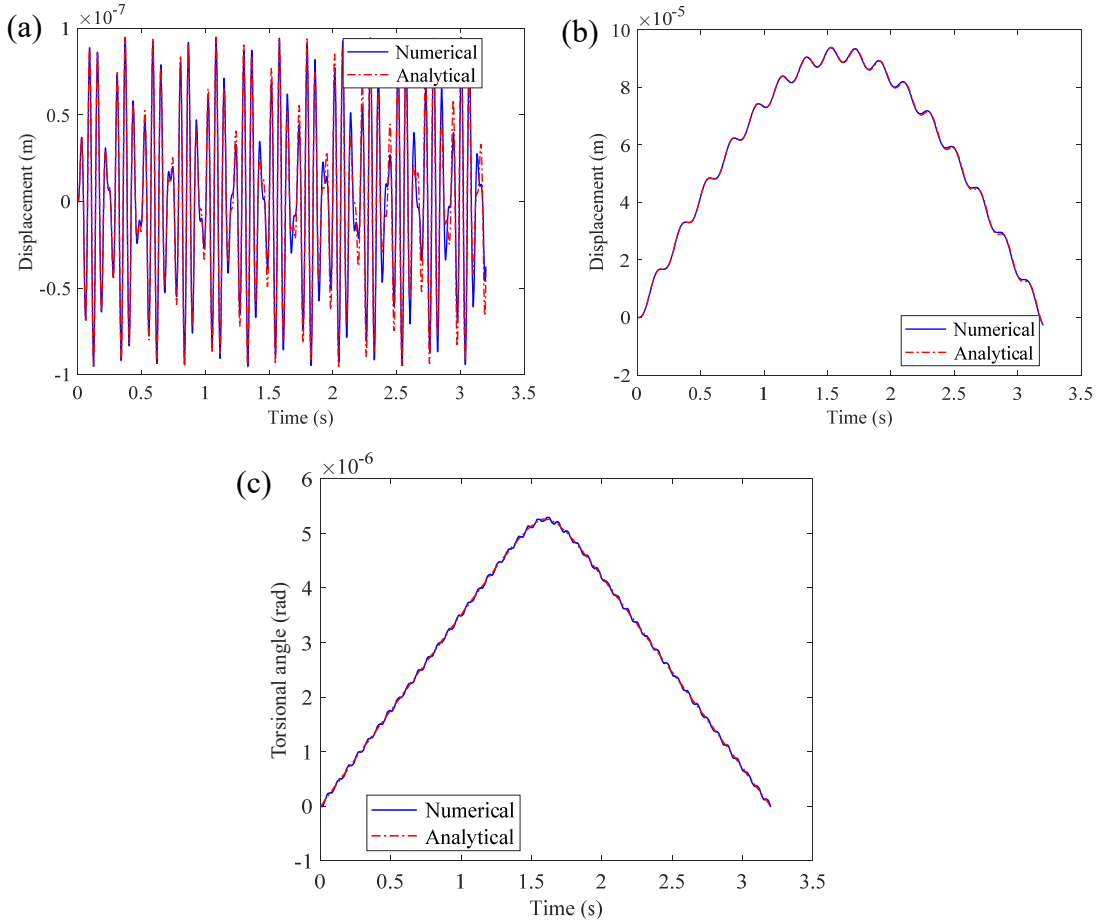

Figure 2. Bridge responses at midspan: (a) lateral, (b) vertical, (c) torsional.

The right- and left-sides accelerations calculated by theory and FEM solutions were compared those obtained backwardly in Figures. 2 and 3, respectively. A good agreement has been achieved between the analytical and FEM solutions in time and frequency domains. This agreement confirms the reliability of the closed-form solution derived in Section 2, together with the procedure for computing the contact response. Of interest is that from the right and left contact spectra of Figure. 2(b) and 3(b), a *large number of frequencies* of the bridge has been "released" via suppression of the vehicle frequencies ω_D^{yv} and $\omega_D^{\theta v}$, or the so-called masking effect. In fact, the frequencies that can be identified for the bridge are not limited to the first four flexural ω_{y1}, ω_{y2}, ω_{y3}, ω_{y4}, and eight "minus" and "plus" torsional-flexural ω_{1^-}, ω_{1^+}, ω_{2^-}, ω_{2^+}, ω_{3^-}, ω_{4^-}, ω_{5^-}, ω_{6^-}, because there are *many more* beyond the

range of the figure shown. Such results coincide well with the derivation of closed-form solutions in Section 2.

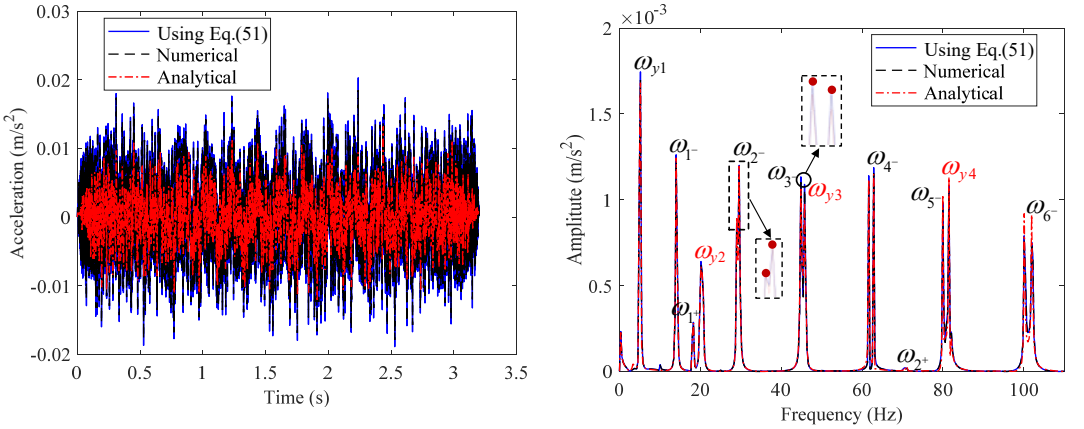

(a) (b)

Figure 2. Right contact accelerations calculated by Eq. (48), theory and FEM: (a) time history, (b) FFT.

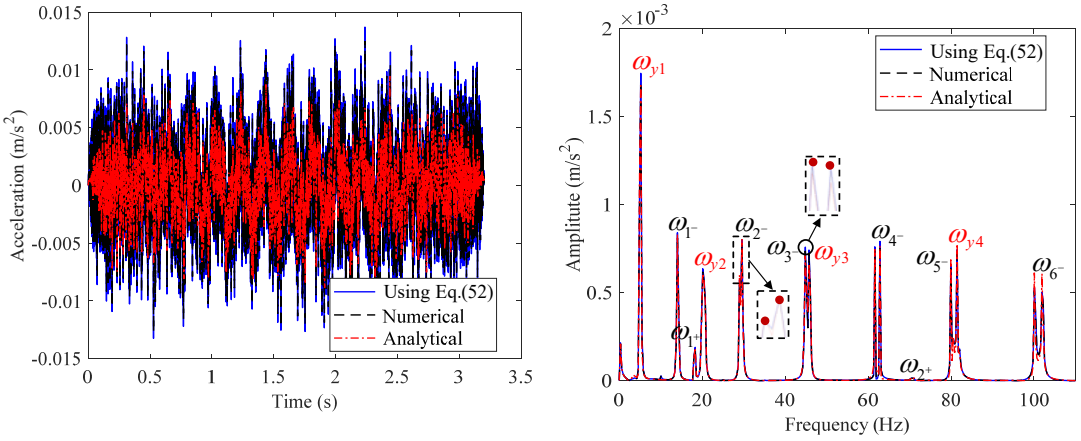

(a) (b)

Figure 3. Left contact accelerations calculated by Eq. (49), theory and FEM: (a) time history, (b) FFT.

4 Conclusions and Contributions

A theory has been presented for retrieving the flexural and flexural-torsional frequencies of thin-walled beams from the rocking motion of the two wheels of a moving test vehicle modeled as a two DOF system. Closed-form solutions have been firstly derived for the vehicle, beam and wheel contact responses. Due to the mono-symmetry of the beam, the torsional-flexural frequencies always appear in conjugate "*minus*" and "*plus*" frequencies in relation to the low- and high-frequency components. The two disturbing factors, i.e., vehicle's self frequencies and bridge's surface roughness, have been eliminated by using the residual contact response of two connected identical vehicles. The reliability of the proposed theory has been validated by the FEM and confirmed in the parametric analysis.

Acknowledgements

This work is supported by National Natural Science Foundation of China (Grant No. 51678091 and 52008060).

References

[1] C. S. Huang, Y. B. Yang, L. Y. Lu, C. H. Chen, Dynamic testing and system identification of a multi-span highway bridge, Earthq. Eng. Struct. Dyn. 28 (8) (1999) 857-878.

[2] H. Li and O.J. Ping, The state of the art in structural health monitoring of cable-stayed bridges, Journal of Civil Structural Health Monitoring. 6(1) (2015) 43-67.

[3] J. P. Yang and B. L. Chen, Rigid-Mass Vehicle Model for Identification of Bridge Frequencies Concerning Pitching Effect. Int. J. Struct. Stab. Dyn. 19(2) (2019): 1950008.

[4] J.T. Li, X.Q. Zhu, S.S. Law, B.J. Samali, Time-varying characteristics of bridges under the passage of vehicles using synchroextracting transform, Mech. Syst. Signal Proc. 140(2020) 106727.

[5] Y. B. Yang, C. W. Lin, and J. D. Yau, Extracting bridge frequencies from the dynamic response of a passing vehicle, J. Sound Vibr. 272(3-5) (2004) 471-493.

[6] Y. B. Yang, J. P. Yang, Zhang B, and Wu YT, Vehicle scanning method for bridge, (John Wiley & Sons, London 2019).